A step-by-step in crystallo guide to bond cleavage and 1,6-anhydro-sugar product synthesis by a peptidoglycan-degrading lytic transglycosylase

Allison H Williams, Richard Wheeler, Lesly Rateau, Christian Malosse, Julia Chamot-Rooke, Ahmed Haouz, Muhamed-Kheir Taha, Ivo G. Boneca

A step-by-step *in crystallo* guide to bond cleavage and 1,6-anhydro-sugar product synthesis by a peptidoglycan-degrading lytic transglycosylase

Received for publication, November 23, 2017, and in revised form, February 12, 2018 Published, Papers in Press, February 26, 2018, DOI 10.1074/jbc.RA117.001095

Allison H. Williams[‡§1], Richard Wheeler[‡§¶], Lesly Rateau[‡§], Christian Malosse[‖], Julia Chamot-Rooke[‖], Ahmed Haouz[**], Muhamed-Kheir Taha[‡‡], and Ivo Gomperts Boneca[‡§2]

From the [‡]Institut Pasteur, Département de Microbiologie, Unité Biologie et Génétique de la Paroi Bactérienne, 75015 Paris, France, [§]INSERM, 75015 Paris, France, the [¶]Gustave Roussy Comprehensive Cancer Center, Tumour Immunology and Immunotherapy, F-94805 Villejuif, France, the [‖]Institut Pasteur, CNRS USR 2000, Unité des Spectrométrie de Masse Structurale et Proteomique, 75015 Paris, France, the [**]Institut Pasteur, Plate-forme de Cristallographie, CNRS-UMR3528, 75724 Paris, France, and the [‡‡]Institut Pasteur, Département d'Infection et Epidémiologie, Unité des Infection Bactériennes Invasives, 75015 Paris, France

Edited by Gerald W. Hart

Lytic transglycosylases (LTs) are a class of enzymes important for the recycling and metabolism of peptidoglycan (PG). LTs cleave the β-1,4-glycosidic bond between *N*-acetylmuramic acid (MurNAc) and GlcNAc in the PG glycan strand, resulting in the concomitant formation of 1,6-anhydro-*N*-acetylmuramic acid and GlcNAc. No LTs reported to date have utilized chitins as substrates, despite the fact that chitins are GlcNAc polymers linked via β-1,4-glycosidic bonds, which are the known site of chemical activity for LTs. Here, we demonstrate enzymatically that LtgA, a non-canonical, substrate-permissive LT from *Neisseria meningitidis* utilizes chitopentaose ($(GlcNAc)_5$) as a substrate to produce three newly identified sugars: 1,6-anhydro-chitobiose, 1,6-anhydro-chitotriose, and 1,6-anhydro-chitotetraose. Although LTs have been widely studied, their complex reactions have not previously been visualized in the crystalline state because macromolecular PG is insoluble. Here, we visualized the cleavage of the glycosidic bond and the liberation of GlcNAc-derived residues by LtgA, followed by the synthesis of atypical 1,6-anhydro-GlcNAc derivatives. In addition to the newly identified anhydro-chitin products, we identified trapped intermediates, unpredicted substrate rearrangements, sugar distortions, and a conserved crystallographic water molecule bound to the catalytic glutamate of a high-resolution native LT. This study enabled us to propose a revised alternative mechanism for LtgA that could also be applicable to other LTs. Our work contributes to the understanding of the mechanisms of LTs in bacterial cell wall biology.

This work was supported by EMBO long-term fellowship ALTF 732-2010 (to A. H. W.), an Institut Carnot-Pasteur Maladies Infectieuses fellowship (to A. H. W.), ERC starting grant (PGN from SHAPE to VIR 202283) (to I. G. B.), Fondation pour la Recherche Médicale (FRM) Grant programme d'urgence (DBF20160635726) (to I. G. B.), Agence National de la Recherche Grant ANR-14-CE14-0003 (to M. K. T.), and Laboratoire d'Excellence "Integrative Biology of Emerging Infectious Diseases" Grant ANR-10-LABX-62-IBEID from the French government's Investissement d'Avenir program. The authors declare that they have no conflicts of interest with the contents of this article.

The atomic coordinates and structure factors (codes 6FPN, 5O1J, 5O29, 5O2N, and 5O24) have been deposited in the Protein Data Bank (http://wwpdb.org/).

This article contains Tables S1 and S2 and Figs. S1–S3.

[1] To whom correspondence may be addressed. E-mail: awilliam@pasteur.fr.

[2] To whom correspondence may be addressed. E-mail: bonecai@pasteur.fr.

Lytic transglycosylases (LTs)[3] degrade peptidoglycan (PG) to produce GlcNAc and 1,6-anhydro-*N*-acetylmuramic acid (1,6-anhydro-MurNAc), a key cytotoxic elicitor of harmful innate immune responses (1). Many bacteria have redundant LTs; for example, *Escherichia coli* has eight identified LTs (MltA, MltB, MltC, MltD, MltE, MltF, MltG, and Slt70). Similarly, *Neisseria* species can potentially express five LTs (LtgA, LtgB, LtgC, LtgD, and LtgE) (2–4). Recent studies have provided insights into the specific roles of LtgA and LtgD in *Neisseria gonorrhoeae* by showing that their primary function is to release PG monomers capable of activating innate immune signaling and ciliated cell death. These studies further demonstrate that LtgA produces cytotoxic PG monomers that are largely taken into the cytoplasm for recycling, whereas LtgD produces PG monomers that are released (5). LtgA and LtgD display unique substrate specificities: unlike other LTs, they can digest synthetic tetrasaccharide dipeptides into disaccharide products (5). These findings imply that LtgA and LtgD are required to release greater amounts of PG monomers during *Neisseria* sp. infection and therefore lack strict substrate specificity.

LTs are classified into four distinct families based on sequence similarity and consensus sequences. The LTs in subfamily 1 share sequence and structural similarity to the goose-type lysozyme (6). Based on the classification of Blackburn and Clarke (6), family 1 can be further subdivided into five subfamilies (1A to 1E) with distinct secondary structures. Despite the secondary structural differences in LTs, the catalytic residues in the active site are fairly well-conserved.

LT activity is vital to the synthesis and remodeling of PG. Previous structural and biochemical studies revealed that LTs utilize a single catalytic glutamate or aspartate in acid/base catalysis (Fig. 1) (7). LTs are inhibited by a β-hexosaminidase inhibitor (NAG-thiazoline) and bulgecin A (7–14). The inhibition of LTs by NAG-thiazoline in particular established a direct link between the formation of a 1,6-anhydro-muramoyl residue and the oxazolinium ion intermediate in stage 1 of the proposed

[3] The abbreviations used are: LT, lytic transglycosylase; PG, peptidoglycan; MurNAc, *N*-acetylmuramic acid; *meso*-DAP, *meso*-diaminopimelic acid; NAG, *N*-acetylglucosamine; CHES, 2-(cyclohexylamino)ethanesulfonic acid.

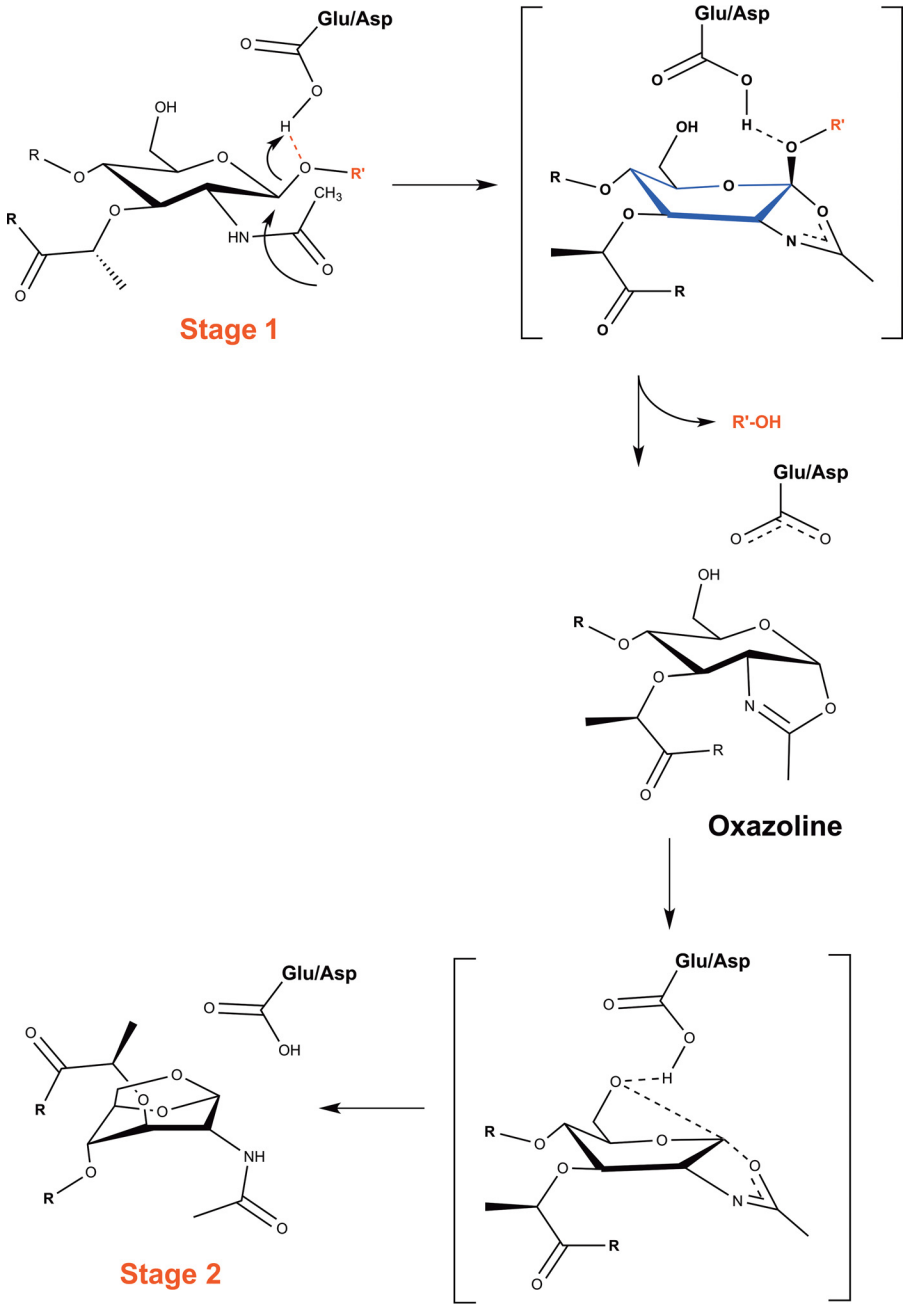

Figure 1. Proposed catalytic mechanism of LTs. LTs use a single catalytic glutamate or aspartate in a simple acid followed by base catalysis. In the absence of a second catalytic residue in the active site, these enzymes proceed via the anchimeric assistance of the MurNAc 2-acetamido group and the formation of the oxazolinium ion intermediate (32).

mechanism (Fig. 1) (7). Because LTs have no known second catalytic residue, the reaction is widely accepted to proceed via the anchimeric assistance of the MurNAc 2-acetamido group and the formation of the oxazolinium ion intermediate (Fig. 1) (7). In stage 2 of the mechanism, the catalytic glutamate acts as a general base to abstract the proton from the C-6-hydroxyl of the MurNAc residue, leading to nucleophilic attack on the anomeric center of the MurNAc residue and the formation of 1,6-anhydro-MurNAc (Fig. 1) (7). The crystal structures of several LTs in complex with non-reactive substrates or product analogs lend support to the proposed mechanism (10, 15–21). Here, we capture an active LT in the crystalline state cleaving the glycosidic bond to (*a*) liberate a single GlcNAc sugar and (*b*) synthesize 1,6-anhydro-GlcNAc-derived products. The signature product of the LT reaction is a 1,6-anhydro-MurNAc derivative. Unexpectedly, LtgA utilized chitopentaose as a substrate and produced 1,6-anhydro-GlcNAc-derived sugars. These high-resolution native structures accompanied by reactions in the crystalline state revealed previously unobserved features and intermediate steps, including, conformational rearrangements of the LT active site during the final stage of 1,6-anhydro-product formation. In the high-resolution native structures of LtgA, a conserved crystallographic water molecule bound to the catalytic glutamate of LtgA was identified. Altogether, this study provides visual insights into how an LT utilizes its substrate during PG metabolism and the conforma-

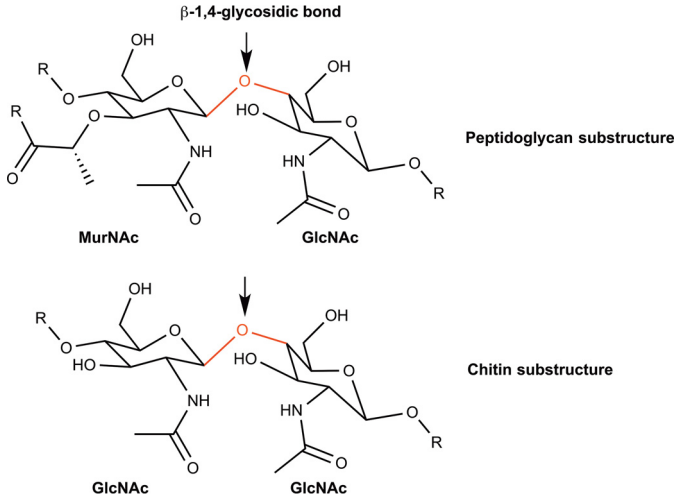

Figure 2. Comparison of the PG and chitin substructures. The β-1,4-glycosidic bond, which is the chemical site of LT activity, occurs in both the PG and chitin substructures.

tional path of the enzyme during catalysis and also sheds light on the likely mechanism of LTs. These insights could impact the development of future antibiotics that target LTs.

Results

Discovery of a lytic transglycosylase with chitinase activity in vitro

Most LTs are inactive toward chito-oligosaccharides, although as a polysaccharide, the chitin polymer mimics the chemical composition of the PG glycan strand (Fig. 2) (22). The β-1,4-glycosidic bond, which is the chemical site of LT activity, is common to the PG and chitin sugar polymer substructures. However, whereas chitin consists of GlcNAc monomers, PG consists of repeating units of MurNAc and GlcNAc. The MurNAc residues linked to the stem peptides are essential to the formation of macromolecular PG and were predicted to be essential to the binding and activity of most LTs.

Serendipitously, we discovered that LtgA can metabolize chitopentaose *in vitro*. HPLC was used to separate the metabolites formed during the cleavage of chitopentaose by LtgA and was coupled with high-resolution MS to determine the chemical structure of the resulting products (Fig. 3, *a* and *b*, and Fig. S1, *a* and *b*). The single peak in the HPLC trace and the mass spectrum of the starting substrate revealed that the ligand was chitopentaose and was not contaminated by other chito-oligosaccharides (Fig. S1, *a* and *b*). LtgA cleaved chitopentaose to yield chitobiose, chitotriose, chitotetraose, and three newly identified products: 1,6-anhydro-chitobiose, 1,6-anhydro-chitotriose, and 1,6-anhydro-chitotetraose (Fig. 3, *a* and *b*, and Fig. S1, *a* and *b*). Although 1,6-anhydro-GlcNAc has not been documented as a product of LTs, LtgA can yield this molecule *in vitro*. To understand the atomic details of how LTs synthesize these anhydro-chitin products and to acquire insights into the LT reaction, we performed crystallographic studies of LtgA complexes.

The structure of native LtgA

Three structures of native LtgA were determined at resolutions of 1.3, 1.4, and 1.85 Å at pH values of 6.5, 7.5 and 9.5, respectively (Tables S1 and S2 and Fig. 4*a*). The overall structure of LtgA is a heart-shaped, highly superhelical configuration consisting of 37 α-helices organized into three domains: U, C, and L (Fig. 4*a*). LTs have very diverse secondary structures, but their catalytic domains are highly conserved (Fig. 4, *a* and *b*, and Fig. S2, *a–d*) (23). LtgA exhibits an overall weak sequence similarity to Slt70 (25%); however, the active site is conserved (Fig. 4, *a* and *b*). The architecture of the active site of LtgA is formed by a total of 10 α-helices (α28, α29, α30, α31, α32, α33, α34, α35, α36, and α37; Fig. S2, *a–d*). A six-helix bundle (α29, α30, α31, α32, α33, and α34) constitutes the active site core, which secures the glycan chain. The proposed catalytic residue Glu^{481} is absolutely conserved in the LT family, whereas Gln^{480}, Val^{492}, Met^{501}, Thr^{504}, Glu^{507}, Asn^{528}, Tyr^{532}, Glu^{580}, Tyr^{551}, Arg^{557}, and Tyr^{584} are highly conserved (Fig. 4, *a* and *b*). LtgA has three *bona fide* saccharide-binding sites (labeled −1 to −3) that form the active site core and two weaker binding sites (labeled −4 and +1) at the entrance and exit of the active site pocket. The majority of the interaction between LTs and the glycan chain would occur within the cleft containing the binding sites −1 to −3 (Fig. 4*c*). Binding site −1 is buried and protected from the solvent and is closest to the previously identified catalytic residue Glu^{481} (Fig. 4*c*). The +1 and −1 subsites represent the catalytic center where LtgA catalyzes the reaction.

Catalysis in crystallo

To visualize the reaction of LtgA at the molecular level, the enzymatic reaction of LtgA was initiated *in crystallo* by soaking a five-moiety glycan sugar (chitopentaose) into native crystals of LtgA grown under crystallization conditions with buffers at pH 6.5, 7.5, and 9.5. At least 30 crystals were monitored over time for the appearance of new density reflecting enzymatic reaction products. The F_oF_c map was compared with the refined native structures of LtgA. In most cases, the native state was retained (Fig. 5*a*), but at the 5-min time point at pH 6.5 and 7.5, we visualized a clear LT reaction intermediate or product.

At pH 7.5, two trapped intermediates (chitotetraose and a GlcNAc sugar) were observed in the active site (Fig. 5*b*). The observed chitotetraose intermediate was trapped in the active site core, whereas a single GlcNAc residue was poised in the departure position at the active site exit (Fig. 5*b*). The chitotetraose intermediate occupied subsites −4 to −1 of the active site (Fig. 4*c*). Cleavage of the glycosidic bond occurred between subsites −1 and +1 (Fig. 5*b*). Remarkably, in the absence of the PG stem peptides, LtgA cleaved a single GlcNAc residue. This behavior had not been observed previously and could not be predicted, because the LT reaction normally produces dimers, trimers, or tetramers when PG is used as a substrate (24). In this intermediate, the GlcNAc residue in the −1 position is significantly distorted and assumes a half-chair position (Fig. 5*b*). The C1-hydroxyl is rotated into the α position (Fig. 1). Notably, the *N*-acetyl of the −1 GlcNAc appears to be mobile, because the electron density surrounding this *N*-acetyl group is sparse (Fig. 5*b*). In the −1 position, the C6-hydroxyl group of the GlcNAc residue is within hydrogen-bonding distance of the (OE2) oxygen of the catalytic residue Glu^{481}. The GlcNAc sugar in the −1 position is further supported in the active site by

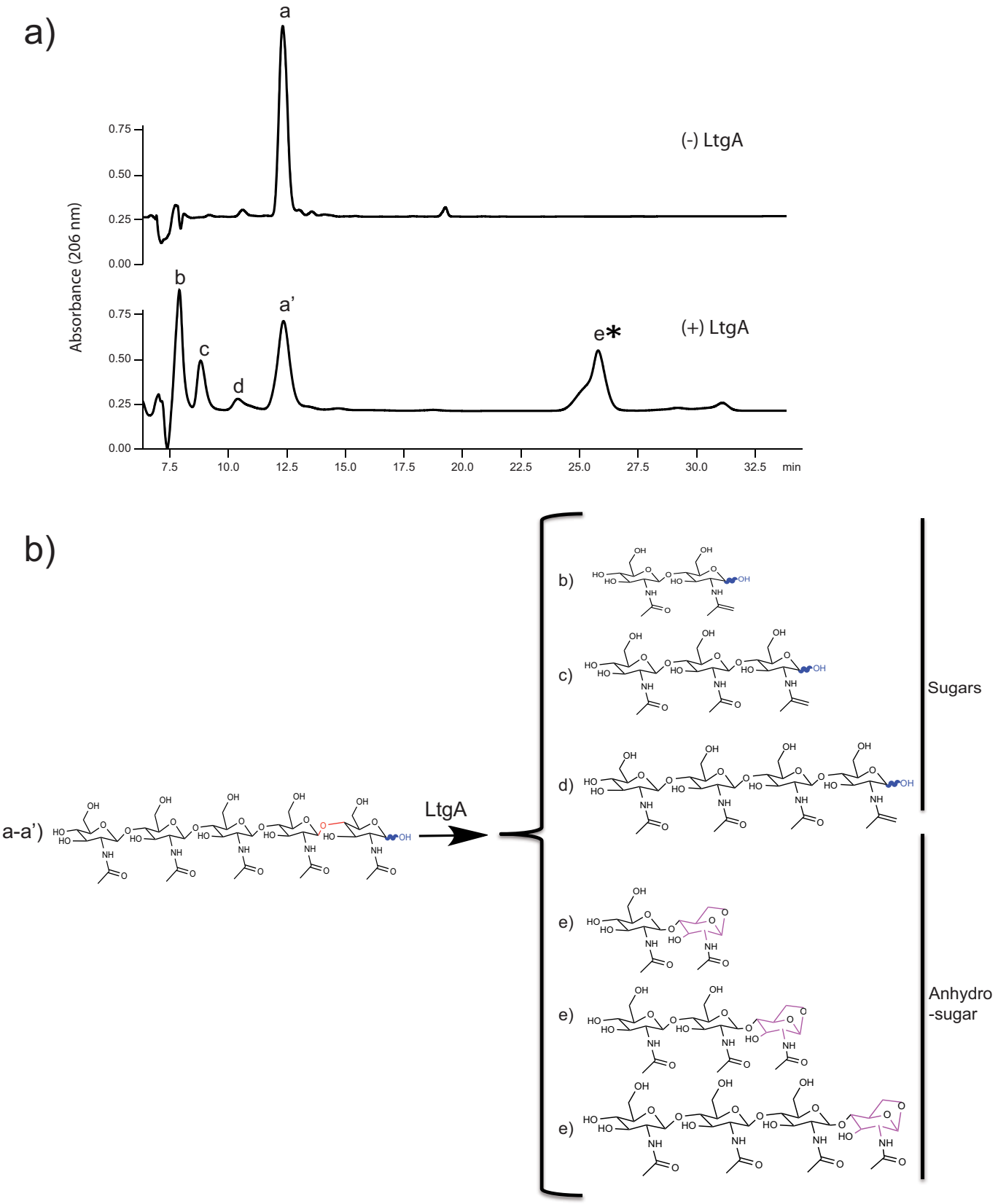

Figure 3. LtgA displays chitin activity. *a*, reversed-phase HPLC results showing that LtgA catalyzes the breakdown of chitopentaose. The peaks are labeled *a*–*e*. *b*, nomenclature of LtgA products identified by MS. Three novel metabolites were identified in *peak e*: 1,6-anhydro-chitobiose (molecular weight, 406.1588), 1,6-anhydro-chitotriose (molecular weight, 609.2344), and 1,6-anhydro-chitotetraose (molecular weight, 812.3203). Most chitobiose (molecular weight, 427.1925) was found in *peak b*, chitotriose (molecular weight, 629.2656) was found in *peak c*, and chitotetraose (molecular weight, 832.3438) was found in *peak d*. Undigested chitopentaose was identified in *peak a'* and the starting substrate in peak a (please see Fig. S1 for detailed MS analyses). The *asterisk* signifies the identification of multiple products in the same peak.

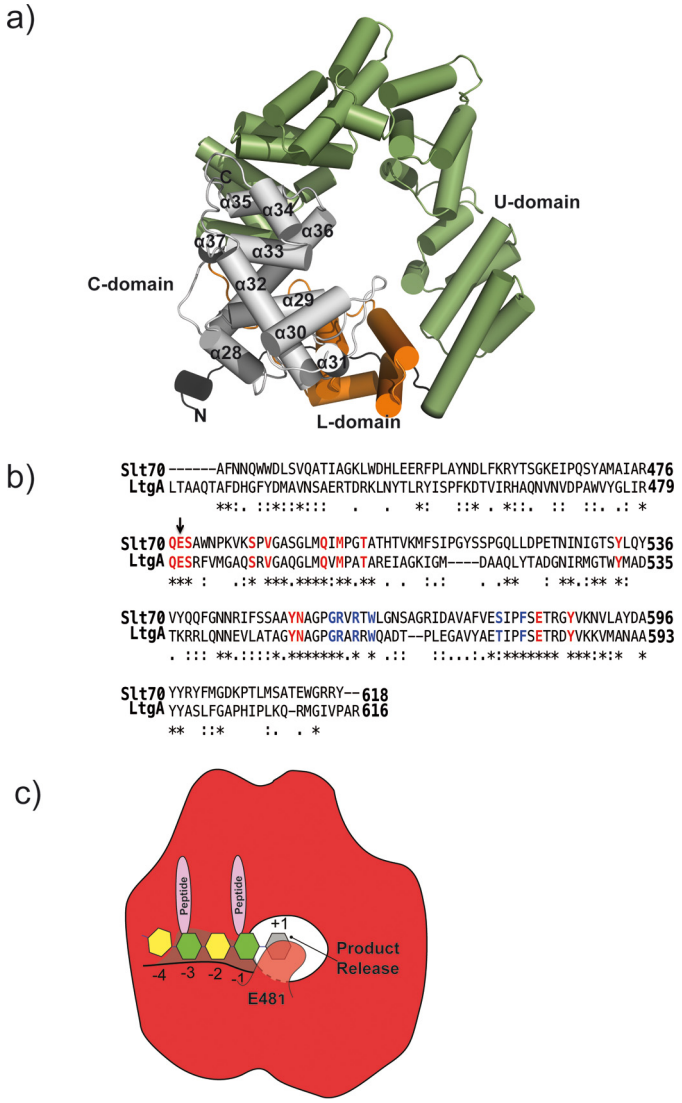

Figure 4. Native structure of LtgA. *a*, ribbon model of the highly helical LtgA structure, consisting of 37 α-helices. LtgA has C (*gray*), L (*orange*), and U (*green*) domains. The C domain houses the catalytic domain. *b*, sequence alignment of the C domains of LtgA and Slt70. Residues predicted to be involved in glycan chain binding and/or catalysis are highlighted in *red*, and residues predicted to be involved in PG stem peptide interactions are highlighted in *blue*. An *arrow* points to the conserved catalytic glutamate of LtgA and Slt70. LtgA shares 25% sequence similarity with the C domain of Slt70. The *asterisk* indicates absolute conservation, and the *dots* (:) indicate high conservation. *c*, three *bona fide* binding subsites lie in the protein interior and are labeled −1 to −3. Subsite −4 is at the entrance of the active site, whereas subsite +1 lies at the exit of the active site. Subsites +1 and −1 are buried and protected from the solvent and are closest to the catalytic residue Glu^{481}. Previous studies predict binding sites −1 and −3 to be occupied by the 1,6-anhydro-MurNAc products.

Asn^{552} and Glu^{580} (Fig. 5*b*). Additionally, Glu^{580} most likely provides structural support for the 2-acetamido group during catalysis. Ser^{490} is hydrogen-bonded to the C1-hydroxyl group of chitotetraose and locks it into the axial position. Tyr^{584} is positioned for direct hydrogen bonding to Glu^{481} and provides a proton relay with the catalytic residue.

As shown in Fig. 5*b*, the C4-hydroxyl group of the departing GlcNAc residue in the +1 position is hydrogen-bonded to the oxygen (OE1) of the catalytic residue (Glu^{481}) (Fig. 5*b*). The nitrogen in the *N*-acetyl group of the +1 GlcNAc is hydrogen-bonded to the backbone oxygen of the catalytic residue, whereas the NE2 of Gln^{480} is hydrogen-bonded to the C6-hydroxyl group. The departing GlcNAc occupies the same space as the GlcNAc sugar that was previously observed in the Slt70–1,6-anhydro-muropeptide product (21). Normally, the glycosidic oxygen is expected to depart with the +1 GlcNAc after bond breaking in the reaction. However, in X-ray data, an extra oxygen atom was observed. This extra oxygen is potentially derived from a water molecule.

In this trapped chitotetraose/GlcNAc intermediate, the distance between the cleaved glycosidic bond (C1-hydroxyl) of chitotetraose and the catalytic residue is precisely 5.4 Å, whereas the C4-hydroxyl group of the departing GlcNAc residue is precisely at hydrogen-bonding distance (2.5 Å) from the catalytic residue. Previous structural studies of *E. coli* LTs, such as MltA, MltC, and MltE, with unreactive glycan strand mimics demonstrated that the catalytic residue is perfectly positioned for its role as a base (2.5–3.0 Å) but is too far (3.6–5.4 Å) from the primary chemistry site (the β-1,4-glycosidic bond) (Fig. S3, *a* and *b*) (11, 25–31). MltA undergoes a drastic conformational change to achieve a nearly productive configuration of the active site (28, 32). However, the structure of MltA with bound chitohexaose demonstrates that the catalytic residue is still distant from the β-1,4-glycosidic bond (32). This distance suggests that further structural rearrangements are necessary for the reaction to proceed. To address this point, we surveyed additional conditions to trap more informative intermediates.

1,6-Anhydro-product formation

At pH 6.5, we observed the formation of 1,6-anhydro-chitotriose with Zn^{2+} directly bound to the catalytic residue Glu^{481} and coordinated by five water molecules. The water-coordinated Zn^{2+} molecule stabilizes the trapped 1,6-anhydro-chitotriose product after the departure of the GlcNAc sugar(s) (Fig. 5*b*). Zn^{2+} was required as an additive to stabilize the native crystals at pH 6.5 but was not required for the activity of LtgA *in vitro* (Fig. 3, *a* and *b*). Additionally, in the native structure of crystals of LtgA grown at pH 6.5, no density corresponding to a Zn^{2+} atom was observed in the active site of LtgA (Fig. 5*a* and Fig. S2).

In this structure, the O6 oxygen of the 1,6-anhydro-GlcNAc product bound in the −1 position is directly hydrogen-bonded to the OE2 of the catalytic residue Glu^{481}. The O7 oxygen of the *N*-acetyl group of the 1,6-anhydro-GlcNAc is directly hydrogen-bonded to Ser^{490}, which was previously involved in locking the C1-hydroxyl group of chitotetraose in the axial position. Overall, the 1,6-anhydro-GlcNAc in the −1 position forms fewer hydrogen-bonding contacts in the active site than the GlcNAc residue in the −1 subsite of the chitotetraose (Fig. 5*b*). For example, the product is no longer hydrogen-bonded to Glu^{580} or Gln^{480} and does not interact directly with Gln^{499} (Fig. 5*b*). The formation of the 1,6-anhydro product represents the final stage of the catalytic mechanism before the product release (Fig. 1). Interestingly, the 1,6 bond of 1,6-anhydro-GlcNAc is now positioned for direct hydrogen bonding to the catalytic residue, signaling overall structural changes in the active site.

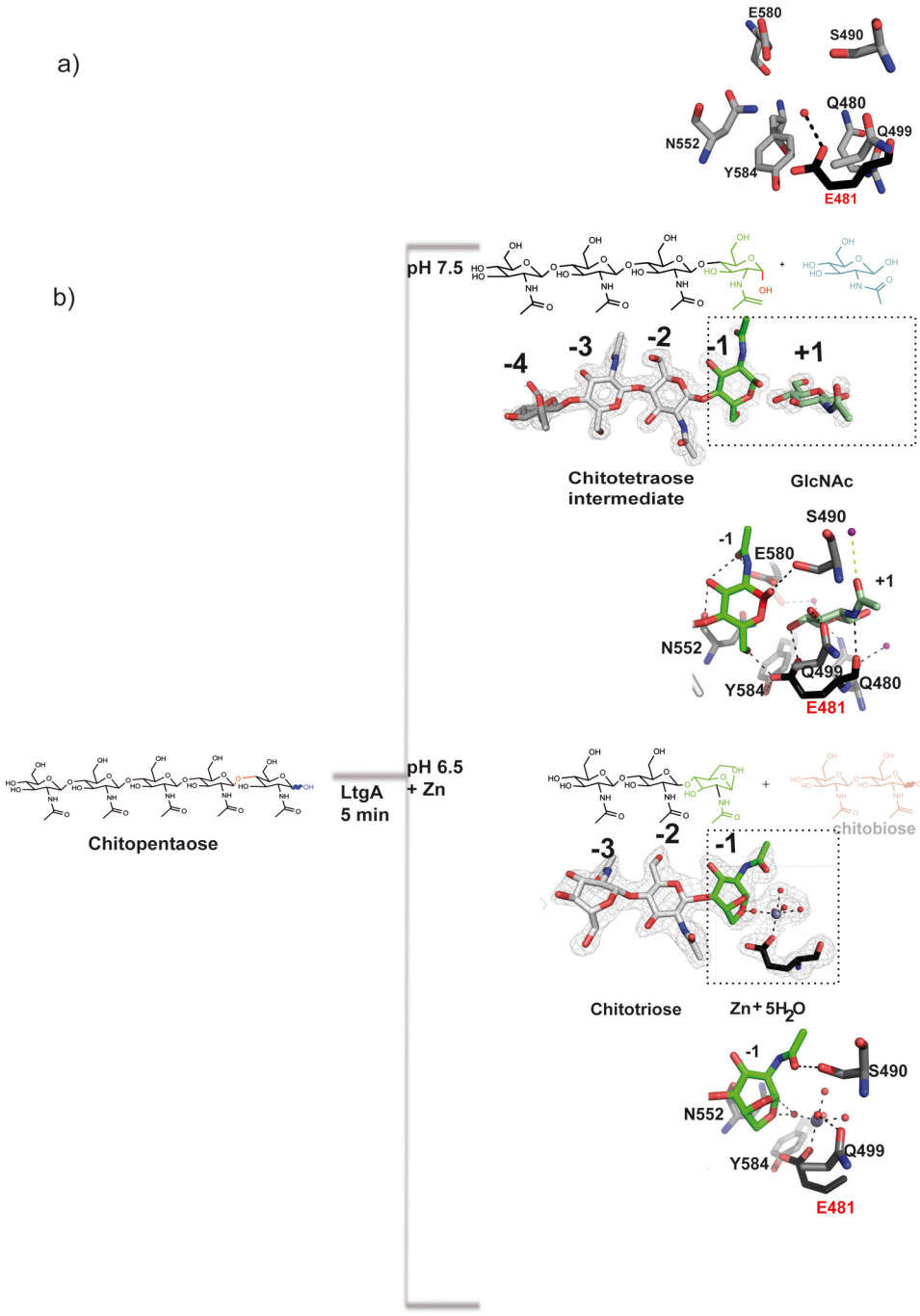

Figure 5. LtgA reaction *in crystallo*. *a*, the catalytic center of LtgA. *b*, trapped intermediates at pH 7.5 and 6.5. The F_oF_c maps colored in *gray* are contoured at 3σ.

Structural rearrangement of the active site of LtgA

The terminal product of the LT reaction is a product containing 1,6-anhydro-muramic acid. To date, all structures of LTs with unreactive glycan chain analogs (MltA-chitohexose, MltE-chitopentaose, and MltC-tetrasaccharide) show distances of 4.66–5.4 Å between the glycosidic bond and the catalytic residue (Fig. S4) (11, 29, 32). Because the substrates in these LT complexes are unreactive, they presumably represent nonproductive enzyme–substrate complexes or mimic the resting state of the enzyme. Therefore, for catalysis to occur, (*a*) elements of the active site must move to bridge the gap, (*b*) glycan sugars must rearrange into a sterically acceptable conformation, or (*c*) the conserved water molecule identified in our native structures must form a proton relay between the glycosidic bond and the catalytic residue, which could enable the reaction to proceed without large active site readjustments (Fig. 6, *a* and *b*, and Fig. S4). With mounting evidence from known structures suggesting a missing link, it was deduced that the highly decorated PG, the natural substrate of LTs, is likely bound in a more catalytically competent manner than unreactive substrate analogs in complexes with LTs. However, in the crystalline state, LtgA, unlike other known LTs, competently

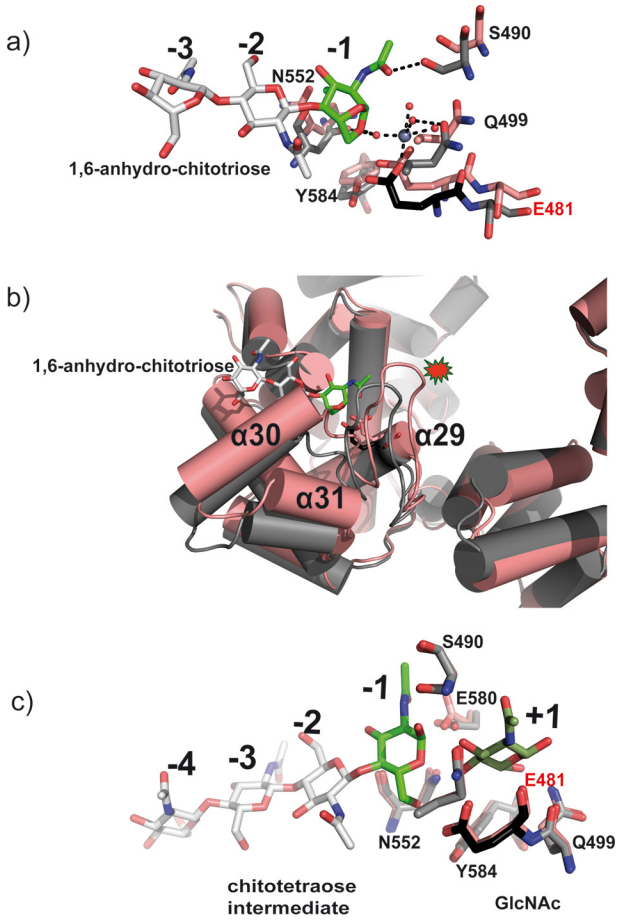

Figure 6. Structural rearrangement of the active site of LtgA following 1,6-anhydro-GlcNAc formation. *a*, superposition of native LtgA (pH 6.5) (*pink*) with the LtgA–1,6-anhydro-GlcNAc intermediate (*gray stick model*). *b*, cartoon model of native LtgA (pH 6.5) (*pink*) superposed on the LtgA–1,6-anhydro-GlcNAc intermediate (*gray stick model*). *c*, native LtgA superposed on the LtgA–chitotetraose–GlcNAc intermediate complex.

degrades chitopentaose to produce 1,6-anhydro-sugars. Surprisingly, the catalytic domain of the LtgA–1,6-anhydro-GlcNAc complex (Fig. 6*a*, *gray*) showed a root mean square deviation of 1.8 Å when superimposed on all other native or trapped complexes (Fig. 6*a*, *pink*). Dramatic localized deviations of 3.2–7.0 Å appeared in the catalytic center (Fig. 6, *a* and *b*). Specifically, significant perturbation occurred in α30, α31, and the loop connecting α29 to α30 (Figs. 2*a* and 6*a*). LtgA is an exolytic enzyme, and in the substrate-bound version, the loop that connects α29 to α30 restricts the number of residues that the active site can accommodate via steric hindrance (Fig. 6*b*). Gln^{499} is on this flexible loop and supports the departing sugar residues in the +1 position (pH 6.5) during catalysis. However, it does not contact the 1,6-anhydro-sugar product. This flexible loop recedes after product formation (Fig. 6*b*). Globally, in product formation mode, the active site is in a more open conformation than in all other forms of LtgA (Fig. 6, *a*–*c*). The more open conformation of the LtgA–1,6-anhydro-GlcNAc complex may facilitate product release.

Overall view of LtgA PG-binding site

LTs are specific for PG as a substrate. The studies herein were conducted in the absence of the PG stem peptide, and therefore, we wanted to obtain a global view of PG binding to LTs. Because substructures of PG that included the stem peptide were unavailable in the quantity and purity necessary for crystallization, a docking model of LtgA–chitotetraose complexed with a tripeptide that terminates in a *meso*-diaminopymelyl (*meso*-DAP) residue was created (Fig. 7).

The majority of the interaction between LTs and chitotetraose occurs at binding sites −1 through −4 (Fig. 5*b*). Binding sites −2 and −4 easily accommodate GlcNAc residues, but the attachment of the PG stem peptides would create significant steric hindrance (Fig. 7). Binding sites −1 and −3 accommodate the MurNAc residues and attached stem peptides (Figs. 5*b* and 7). A groove that can accommodate the stem peptide core extends from binding sites −1 and −3. Moreover, binding site −1 is aligned with conserved residues that were previously identified in Slt70 to be crucial for PG stem peptide binding (22). These residues are conserved in LtgA (Figs. 3*b* and 5*b*).

The docked stem peptides bound in binding sites −1 and −3 are flanked by the highly conserved residues Glu^{580}, Phe^{578}, Thr^{575}, Trp^{561}, and Arg^{559} (Fig. 7). This putative binding site of PG stem peptides was previously inferred from the high-resolution crystal structure of Slt70 complexed with 1,6-anhydro-murotripeptide (22).

Discussion

This study has captured LtgA in action and provides the first visual snapshots of how LTs liberate 1,6-anhydro-MurNAc and GlcNAc products. LtgA snapshots were captured both with LtgA in its native form and as it liberated a GlcNAc residue with chitotetraose in the process of forming 1,6-anhydro-chitotetraose (Fig. 5*b*). In our assay, we identified chitotetraose and 1,6-anhydro-chitotetraose as reaction products but did not observe free single GlcNAc (Fig. 3, *a* and *b*). We postulate that GlcNAc was eluted close to the void volume of the column in our HPLC analysis and therefore did not appear as a defined, mono-species peak (Fig. 3, *a* and *b*). The sugar rings are well-adapted to the shape of the active site, where subsites −1, −2, and −3 are locked in the interior of the protein, whereas +1 and −4 are more flexible on the edges. The flexibility and orientation of GlcNAc in the +1 position would allow unobstructed exit from the active site after cleavage.

In the reported structures of LT complexes with bound substrate analogs to date, the glycosidic bond and catalytic residues are outside hydrogen-bonding range. In the LtgA–1,6-anhydro-chitotriose complex, before product expulsion, we observed localized rearrangement of the active site (Fig. 5*c*). A possible explanation for this phenomenon is that the LT active site undergoes conformational changes that bring the catalytic residue within hydrogen-bonding distance of the glycosidic bond. However, this rearrangement during the initiation steps (stage 1) of the reaction (Fig. 1) was not observed in this study or in other studies where LTs were crystallized with inactive substrate analogs (22).

Unexpectedly, a conserved crystallographic water molecule was perfectly poised in the native complex to perform a proton relay between residue Glu^{481} and the glycosidic bond (Fig. 5*a* and Fig. S3). This relay would ease the need for the substrate or active site to undergo drastic conformation changes to initiate

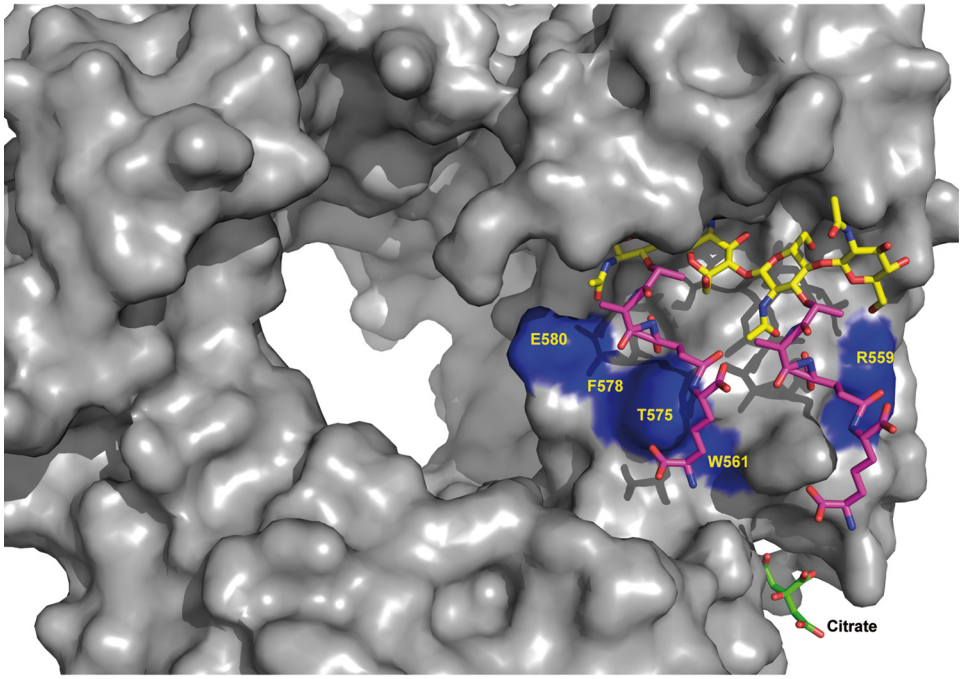

Figure 7. Model of the interaction between LtgA and chitotetraose modified with PG tripeptide stems, which terminates in a *meso*-DAP residue, MurNAc(L-Ala-D-Glu-*meso*-DAP). The model highlights the two stem peptide-binding grooves predicted to be involved in PG binding for *E. coli* Slt70, aligned on the conserved residues (Glu^{580}, Phe^{578}, Thr^{575}, Trp^{561}, and Arg^{559}) (Fig. 4*b*). A citrate molecule (colored in *pink*) occupies binding site −2.

the reaction in stage 1 (Fig. 1). Thus, LtgA and quite possibly other LTs could operate via a water-mediated substrate-assisted catalytic mechanism. In this mechanism, Glu^{580} is positioned to provide structural support to the negative charge of the 2-acetamido (Figs. 5, *a* and *b*, and 8). During bond cleavage, the water molecule serves as a proton relay to the glycosidic bond and supports the formation of an oxazolium intermediate that deprotonates the catalytic residue Glu^{481} (Fig. 8). Glu^{481} then acts as a general base to abstract a proton from the C6-OH of the MurNAc residue, thereby allowing the intramolecular nucleophilic attack of the C1, which disrupts the oxazoline intermediate and forms the reaction products (Fig. 8).

LtgA is the first documented case of an LT that not only degrades chitin sugars but is also able to cleave a single sugar residue from the polymeric substrate. Normally, when LTs degrade the PG, the minimal product cleaved from the polymeric PG is a peptide-linked disaccharide (7). Interestingly, lysozyme, a glycosidase that is closely related to the LTs, also cleaves chitin sugar, releasing a single residue at a time (33). When LTs cleave their substrate, they utilize a single catalytic residue, and the reaction proceeds via the anchimeric assistance of the MurNAc 2-acetamido group and the formation of the oxazolinium ion intermediate (7). Lysozyme utilizes a different mechanism, whereby two catalytic residues serve the role of a general acid/base, and the documented intermediate steps include the formation and subsequent break down of a covalent glycosyl-enzyme intermediate (34, 35). In the mechanism of lysozyme, there is inversion of the sugar configuration surrounding the anomeric carbon at each step; however, there is a net retention of the stereochemistry when the product is formed. Crystallographic studies of an active lysozyme (hen egg-white lysozyme) in the presence of a chitin sugar have revealed that the equivalent sugar in subsite −1 is distorted and

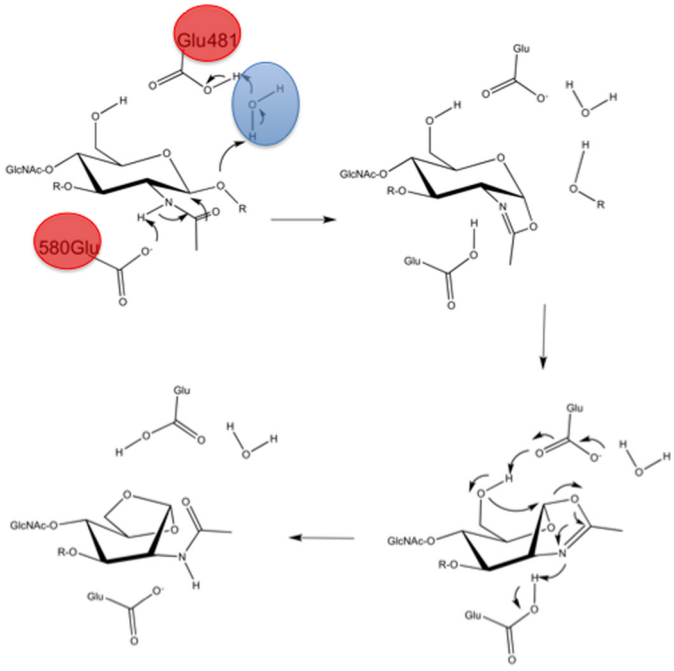

Figure 8. Revised LT mechanism. Glu^{481} is the sole catalytic residue. The 2-acetoamido group of GlcNAc may serve as an intramolecular nucleophile that is supported by Glu^{580}. An intermediate water molecule serves as a proton relay between the glycosidic bond and Glu^{481}, which activates the C6 hydroxyl group as a general base and cleaves the glycosidic bond.

assumes a half-chair position (35). The mechanism of family 18 chitinases is similar to LtgA and other LTs (36). These chitinases mechanistically utilize substrate participation or anchimeric assistance and cycle through an oxazolinium ion intermediate. However, similar to lysozyme, the stereochemical configuration around the anomeric carbon changes

but retains the original configuration after the product formation step.

In the LtgA–chitotetraose plus GlcNAc complex, each pyranose ring of all the GlcNAc residues in the five subsites, (−4, −3, −2, −1, and +1) adopts a chair conformation (Fig. 5*b*). Surprisingly, ring inversion of the GlcNAc residue was only observed in subsite −3 of the final product complex (LtgA–1,6-anhydro-chitotriose). Subsite −3 is distal from the catalytic center (subsite −1 and +1), and the GlcNAc residue appears to assume a twisted boat conformation (Fig. 5*b*). Because there was also structural rearrangement of the LtgA active site after the 1,6-anhydro product formation, subsite −3 possibly selected a different conformer of the GlcNAc residue because of changes in binding energy between the GlcNAc residue and LtgA (Fig. 6, *a–c*).

LtgA degrades both chito-oligosaccharides and PG (Fig. 5, *a* and *b*) (5). Additionally, docking studies suggest no direct role of the stem peptides in the LtgA reaction (Fig. 7); however, they probably play a direct role in enzyme-substrate specificity. Structurally, the active site of LtgA is identical to that of *E. coli* Slt70 (Figs. 3*b* and 5*b*). However, there are subtle differences between the overall structures of Slt70 and LtgA. For example, LtgA has a long membrane-bound N termini that attaches itself to the membrane, whereas Slt70 remains localized in the periplasm (Fig. 4*a*) (5). This structural difference could affect the utilization of substrates *in vitro*. Overall, LtgA appears to be more permissive in its substrate utilization than other reported LTs.

The identification of 1,6-anhydro-chitotriose in the active site is the first snapshot taken of an LT synthesizing a 1,6-anhydro-sugar in the crystalline state. The F_oF_c maps contoured at 3σ clearly showed the 1,6-anhydro-chitotriose, illustrating the path that the GlcNAc follows to facilitate the formation of the 1,6-anhydro-sugar. Interestingly, the sugar residue in the −3 position of the 1,6-anhydro-GlcNAc products appears to adopt a twisted boat conformation, suggesting that the glycan strand undergoes multiple conformational changes during the catalytic breakdown of chitopentaose.

These findings reported here reveal snapshots of intermediate steps in the LtgA reaction and provide unprecedented insight into how LTs cleave the glycosidic bond and form cytotoxic PG fragments. The results also suggest an alternative mechanism that could resolve previous discrepancies regarding the initiation of the LT reaction mechanism. Additionally, these trapped intermediates reveal informative details such as loop rearrangements, domain motion, substrate conformation, and transition state stabilization, which are all hallmarks of an active enzyme in motion. This study further emphasizes the pivotal role of LTs in PG biology, and the atomic-level insights into the studied mechanism should facilitate the design of universal inhibitors or antibiotics that target the LT family.

Experimental procedures

X-ray crystallography

Crystallization screening was conducted by the sitting drop vapor diffusion method with a Mosquito® (TTP Labtech) automated crystallization system. All crystals of native LtgA (15–20 mg/ml) were grown at 18 °C and appeared within 2–3 days. Native LtgA was crystallized under three different conditions using a 1:1 (v/v) ratio against the following well solutions: (*a*) 100 mM CHES, pH 9.5, 100 mM trisodium citrate, and 30% (w/v) PEG 3000; (*b*) 33% (w/v) PEG 6000 and 100 mM HEPES, pH 7.5; or (*c*) 0.2 M zinc acetate, 0.1 M sodium cacodylate, pH 6.5, and 0.1 M 18% (w/v) PEG 8000. The crystals were rectangular in shape and grew to ~200–300 microns in length. Crystals of selenomethionine-labeled LtgA were grown at 18 °C in a 1:1 (v/v) ratio against a well solution containing 0.01 M trisodium citrate, 33% (w/v) PEG 6000 and HEPES, pH 7.5. To initiate the reactions, crystals were soaked with a 10-fold molar excess of chitopentaose over the course of an hour (5, 15, 30, 45, and 60 min) at pH 6.5, 7.5, and 9.5 before flash-cooling. The crystals were cryoprotected in a mixture of 50% Paratone and 50% paraffin oils and flash-cooled in liquid nitrogen.

Single-wavelength anomalous dispersion diffraction data were collected at the selenium absorption peak at the Soleil Synchrotron (Beamline Proxima-1). The highest-resolution selenomethionine crystals diffracted to 1.5 Å with anomalous signal to 1.8 Å (Tables S1 and S2). The initial phases were found using Shelxc/d/e, and the initial model was built using PHENIX autobuild with 13 selenium sites and a figure of merit of 0.70 (37, 38). The refined single-wavelength anomalous dispersion structure was used to determine the phases for the native data set. Data processing for all structures was performed using XDS (39). Molecular replacement was performed using PHENIX (37). Building was conducted using Coot (40), and restrained refinement was carried out using a combination of PHENIX and the ccp4 software suite (37, 41). MolProbity was used for iterative structure improvements during building and refinement (42).

All structural figures were generated using PyMOL (the PyMOL Molecular Graphics System, version 1.5; Schrödinger). The crystallographic parameters, data statistics, and refinement statistics are shown in Table S1. The coordinates and structure factors of native LtgA, and LtgA intermediates have been deposited in the Protein Data Bank with the accession codes 6FPN, 501J, 5029, 502N, and 5024.

Docking studies

The LtgA chitotetraose complex was modified with PG tripeptide stems terminating in a *meso*-DAP residue, *i.e.* MurNAc(L-Ala-D-Glu-*meso*-DAP). The docking and alignments were performed in Coot. The full LtgA–chitotetraose–meso-DAP complex was refined against the structure factors of the LtgA–chitotetraose complex using the ccp4 software refmac (40). The complex was evaluated and modified in Coot to improve the chemical accuracy.

Protein expression and purification

All constructs were created using standard molecular biology techniques as previously described (14). All constructs used in this study were GST fusions from pGEX-4T1 (GE Lifesciences). The native LtgA protein was expressed following transformation of the recombinant plasmids into BL21(DE3) Gold competent cells (Novagen). Protein expression was induced when the cells reached an optical density at 600 nm with 0.6 mM isopropyl

β-D-thiogalactopyranoside at an optical density of 0.7–0.8, and harvest was performed after 4 h postinduction with cultures grown at 18 °C. Selenomethionine-labeled proteins were expressed in B834 (DE3) and then grown in autoinduction media as described by Studier (43). After glutathione affinity chromatography and thrombin cleavage, the proteins were purified to homogeneity by size exclusion chromatography (Superdex 200; GE Healthcare) in 50 mM HEPES, pH 7.4, 150 mM NaCl, and 1 mM β-mercaptoethanol. After gel filtration, the proteins were immediately used for crystallization. Alternatively, the proteins were flash frozen in liquid nitrogen and stored at −80 °C.

LtgA chitopentaose reaction

LtgA activity with chitopentaose was assessed using synthetic chitopentaose (Carbosynth) and purified LtgA. The chitopentaose (10 μM) was incubated in the presence of 1.4 μM of LtgA in 12.5 mM sodium phosphate buffer, pH 5.6, at 37 °C for 5 min. Control reactions lacking chitopentaose or enzyme were also performed. The total reaction volume was 200 μl. After 5 min of incubation at 37 °C, the reaction was stopped by incubating the samples in a boiling water bath for 3 min. The enzymatic reaction products were separated by reversed-phase HPLC using a Shimadzu LC-20 system with a Hypersil GOLD aQ column (250 × 4.6 mm, 5-μm particle size, flow rate of 0.5 ml/min at 52 °C; Thermo Fisher Scientific). The mobile phase gradient was H_2O + 0.05% trifluoroacetic acid with a 0–25% acetonitrile gradient over 135 min. Chito-oligosaccharide peaks were collected and dehydrated by vacuum centrifugation. A full-spectrum MS scan was obtained on the LTQ Velos Orbitrap at a resolution of 60,000. Collected fractions were further analyzed in positive ion mode by direct nanoelectrospray infusion using a Tri-Versa Nanomate (Advion Biosciences) on an LTQ Velos Orbitrap mass spectrometer equipped with an electron transfer dissociation (ETD) module (Thermo Fisher Scientific). A full set of automated positive ion calibrations was performed immediately before mass measurement. All spectra were acquired in full profile mode. For the MS experiments, the ions were accumulated in the ion trap and then transferred to the Orbitrap for high-resolution mass measurement. For the MS/MS experiments, ions were selected with an appropriate mass window, and higher-energy collisional dissociation was performed at normalized collision energies of 15–25%, with other activation parameters set to default values. The spectra were acquired in the Fourier transform-based mass spectrometer over several minutes with five microscans and a resolution of 60,000 for MS and 30,000 of m/z 400 for MS/MS before being processed with Thermo Xcalibur 2.2. Multiply charged ion spectra were deconvoluted using Xtract.

Author contributions—A. H. W. and I. G. B. conceptualization; A. H. W., R. W., A. H., and I. G. B. data curation; A. H. W., R. W., J. C.-R., M.-K. T., and I. G. B. formal analysis; A. H. W. and I. G. B. validation; A. H. W., R. W., L. R., C. M., and A. H. investigation; A. H. W. and R. W. methodology; A. H. W. wrote the paper; A. H. W and I. G. B supervision; A. H. and M.-K. T. resources; M.-K. T. and I. G. B. funding acquisition; I. G. B. project administration; I. G. B. writing-review and editing.

Acknowledgments—We thank the staff at beamlines PX1 and PX2 at SOLEIL synchrotron (Saclay, France), at beamline ID29 of the European Synchrotron Radiation Facility (Grenoble, France) and at beamline X06DA of the Swiss Light Source synchrotron (Villigen, Switzerland). We thank Dr. Yves Janin for careful review of the chemical structures. We are eternally grateful to Frederick Saul, Patrick Weber, and Marco Bellinzoni for advice and assistance. We thank Dr. Stephen Lory for helpful criticism, comments, and edits.

References

1. Viala, J., Chaput, C., Boneca, I. G., Cardona, A., Girardin, S. E., Moran, A. P., Athman, R., Mémet, S., Huerre, M. R., Coyle, A. J., DiStefano, P. S., Sansonetti, P. J., Labigne, A., Bertin, J., Philpott, D. J., *et al.* (2004) Nod1 responds to peptidoglycan delivered by the Helicobacter pylori cag pathogenicity island. *Nat. Immunol.* **5,** 1166–1174 CrossRef Medline
2. Kohler, P. L., Hamilton, H. L., Cloud-Hansen, K., and Dillard, J. P. (2007) AtlA functions as a peptidoglycan lytic transglycosylase in the *Neisseria gonorrhoeae* type IV secretion system. *J. Bacteriol.* **189,** 5421–5428 CrossRef Medline
3. Cloud-Hansen, K. A., Hackett, K. T., Garcia, D. L., and Dillard, J. P. (2008) *Neisseria gonorrhoeae* uses two lytic transglycosylases to produce cytotoxic peptidoglycan monomers. *J. Bacteriol.* **190,** 5989–5994 CrossRef Medline
4. Chan, Y. A., Hackett, K. T., and Dillard, J. P. (2012) The lytic transglycosylases of *Neisseria gonorrhoeae*. *Microb. Drug Resist.* **18,** 271–279 CrossRef Medline
5. Schaub, R. E., Chan, Y. A., Lee, M., Hesek, D., Mobashery, S., and Dillard, J. P. (2016) Lytic transglycosylases LtgA and LtgD perform distinct roles in remodeling, recycling and releasing peptidoglycan in *Neisseria gonorrhoeae*. *Mol. Microbiol.* **102,** 865–881 CrossRef Medline
6. Blackburn, N. T., and Clarke, A. J. (2001) Identification of four families of peptidoglycan lytic transglycosylases. *J. Mol. Evol.* **52,** 78–84 CrossRef Medline
7. Reid, C. W., Blackburn, N. T., Legaree, B. A., Auzanneau, F. I., and Clarke, A. J. (2004) Inhibition of membrane-bound lytic transglycosylase B by NAG-thiazoline. *FEBS Lett.* **574,** 73–79 CrossRef Medline
8. Templin, M. F., Edwards, D. H., and Höltje, J. V. (1992) A murein hydrolase is the specific target of bulgecin in *Escherichia coli*. *J. Biol. Chem.* **267,** 20039–20043 Medline
9. Thunnissen, A. M., Rozeboom, H. J., Kalk, K. H., and Dijkstra, B. W. (1995) Structure of the 70-kDa soluble lytic transglycosylase complexed with bulgecin A: implications for the enzymatic mechanism. *Biochemistry* **34,** 12729–12737 CrossRef Medline
10. van Asselt, E. J., Kalk, K. H., and Dijkstra, B. W. (2000) Crystallographic studies of the interactions of *Escherichia coli* lytic transglycosylase Slt35 with peptidoglycan. *Biochemistry* **39,** 1924–1934 CrossRef Medline
11. Fibriansah, G., Gliubich, F. I., and Thunnissen, A. M. (2012) On the mechanism of peptidoglycan binding and cleavage by the endo-specific lytic transglycosylase MltE from *Escherichia coli*. *Biochemistry* **51,** 9164–9177 CrossRef Medline
12. Bonis, M., Williams, A., Guadagnini, S., Werts, C., and Boneca, I. G. (2012) The effect of bulgecin A on peptidoglycan metabolism and physiology of *Helicobacter pylori*. *Microb. Drug Resist.* **18,** 230–239 CrossRef Medline
13. Skalweit, M. J., and Li, M. (2016) Bulgecin A as a beta-lactam enhancer for carbapenem-resistant *Pseudomonas aeruginosa* and carbapenem-resistant *Acinetobacter baumannii* clinical isolates containing various resistance mechanisms. *Drug Des. Devel. Ther.* **10,** 3013–3020 CrossRef Medline
14. Williams, A. H., Wheeler, R., Thiriau, C., Haouz, A., Taha, M. K., and Boneca, I. G. (2017) Bulgecin A: the key to a broad-spectrum inhibitor that targets lytic transglycosylases. *Antibiotics* (*Basel*) **6,** E8 CrossRef Medline
15. Lommatzsch, J., Templin, M. F., Kraft, A. R., Vollmer, W., and Höltje, J. V. (1997) Outer membrane localization of murein hydrolases: MltA, a third lipoprotein lytic transglycosylase in *Escherichia coli*. *J. Bacteriol.* **179,** 5465–5470 CrossRef Medline

16. Engel, H., Smink, A. J., van Wijngaarden, L., and Keck, W. (1992) Murein-metabolizing enzymes from *Escherichia coli*: existence of a second lytic transglycosylase. *J. Bacteriol.* **174,** 6394–6403 CrossRef Medline
17. Dijkstra, A. J., Hermann, F., and Keck, W. (1995) Cloning and controlled overexpression of the gene encoding the 35 kDa soluble lytic transglycosylase from *Escherichia coli*. *FEBS Lett.* **366,** 115–118 CrossRef Medline
18. van Asselt, E. J., and Dijkstra, B. W. (1999) Binding of calcium in the EF-hand of *Escherichia coli* lytic transglycosylase Slt35 is important for stability. *FEBS Lett.* **458,** 429–435 CrossRef Medline
19. van Asselt, E. J., Dijkstra, A. J., Kalk, K. H., Takacs, B., Keck, W., and Dijkstra, B. W. (1999) Crystal structure of *Escherichia coli* lytic transglycosylase Slt35 reveals a lysozyme-like catalytic domain with an EF-hand. *Structure* **7,** 1167–1180 CrossRef Medline
20. Leung, A. K., Duewel, H. S., Honek, J. F., and Berghuis, A. M. (2001) Crystal structure of the lytic transglycosylase from bacteriophage lambda in complex with hexa-N-acetylchitohexaose. *Biochemistry* **40,** 5665–5673 CrossRef Medline
21. van Asselt, E. J., Thunnissen, A. M., and Dijkstra, B. W. (1999) High resolution crystal structures of the *Escherichia coli* lytic transglycosylase Slt70 and its complex with a peptidoglycan fragment. *J. Mol. Biol.* **291,** 877–898 CrossRef Medline
22. Romeis, T., Vollmer, W., and Höltje, J. V. (1993) Characterization of three different lytic transglycosylases in *Escherichia coli*. *FEMS Microbiol. Lett.* **111,** 141–146 CrossRef Medline
23. Vollmer, W., Joris, B., Charlier, P., and Foster, S. (2008) Bacterial peptidoglycan (murein) hydrolases. *FEMS Microbiol. Rev.* **32,** 259–286 CrossRef Medline
24. Fukamizo, T., Minematsu, T., Yanase, Y., Hayashi, K., and Goto, S. (1986) Substrate size dependence of lysozyme-catalyzed reaction. *Arch. Biochem. Biophys.* **250,** 312–321 CrossRef Medline
25. Höltje, J. V. (1996) Lytic transglycosylases. *EXS* **75,** 425–429 Medline
26. Scheurwater, E., Reid, C. W., and Clarke, A. J. (2008) Lytic transglycosylases: bacterial space-making autolysins. *Int. J. Biochem. Cell Biol.* **40,** 586–591 CrossRef Medline
27. van Straaten, K. E., Dijkstra, B. W., Vollmer, W., and Thunnissen, A. M. (2005) Crystal structure of MltA from *Escherichia coli* reveals a unique lytic transglycosylase fold. *J. Mol. Biol.* **352,** 1068–1080 CrossRef Medline
28. Powell, A. J., Liu, Z. J., Nicholas, R. A., and Davies, C. (2006) Crystal structures of the lytic transglycosylase MltA from *N. gonorrhoeae* and *E. coli*: insights into interdomain movements and substrate binding. *J. Mol. Biol.* **359,** 122–136 CrossRef Medline
29. Artola-Recolons, C., Lee, M., Bernardo-García, N., Blázquez, B., Hesek, D., Bartual, S. G., Mahasenan, K. V., Lastochkin, E., Pi, H., Boggess, B., Meindl, K., Usón, I., Fisher, J. F., Mobashery, S., and Hermoso, J. A. (2014) Structure and cell wall cleavage by modular lytic transglycosylase MltC of *Escherichia coli*. *ACS Chem. Biol.* **9,** 2058–2066 CrossRef Medline
30. Artola-Recolons, C., Carrasco-López, C., Llarrull, L. I., Kumarasiri, M., Lastochkin, E., Martínez de Ilarduya, I., Meindl, K., Usón, I., Mobashery, S., and Hermoso, J. A. (2011) High-resolution crystal structure of MltE, an outer membrane-anchored endolytic peptidoglycan lytic transglycosylase from *Escherichia coli*. *Biochemistry* **50,** 2384–2386 CrossRef Medline
31. Artola-Recolons, C., Llarrull, L. I., Lastochkin, E., Mobashery, S., and Hermoso, J. A. (2011) Crystallization and preliminary X-ray diffraction analysis of the lytic transglycosylase MltE from *Escherichia coli*. *Acta Crystallogr. Sect. F Struct. Biol. Cryst. Commun.* **67,** 161–163 CrossRef Medline
32. van Straaten, K. E., Barends, T. R., Dijkstra, B. W., and Thunnissen, A. M. (2007) Structure of *Escherichia coli* Lytic transglycosylase MltA with bound chitohexaose: implications for peptidoglycan binding and cleavage. *J. Biol. Chem.* **282,** 21197–21205 CrossRef Medline
33. Fukamizo, T., Torikata, T., Kuhara, S., and Hayashi, K. (1982) Human lysozyme-catalyzed reaction of chitooligosaccharides. *J. Biochem.* **92,** 709–716 CrossRef Medline
34. Kirby, A. J. (2001) The lysozyme mechanism sorted: after 50 years. *Nat. Struct. Biol.* **8,** 737–739 CrossRef Medline
35. Vocadlo, D. J., Davies, G. J., Laine, R., and Withers, S. G. (2001) Catalysis by hen egg-white lysozyme proceeds via a covalent intermediate. *Nature* **412,** 835–838 CrossRef Medline
36. Monzingo, A. F., Marcotte, E. M., Hart, P. J., and Robertus, J. D. (1996) Chitinases, chitosanases, and lysozymes can be divided into procaryotic and eucaryotic families sharing a conserved core. *Nat. Struct. Biol.* **3,** 133–140 CrossRef Medline
37. Adams, P. D., Afonine, P. V., Bunkóczi, G., Chen, V. B., Davis, I. W., Echols, N., Headd, J. J., Hung, L. W., Kapral, G. J., Grosse-Kunstleve, R. W., McCoy, A. J., Moriarty, N. W., Oeffner, R., Read, R. J., Richardson, D. C., *et al.* (2010) PHENIX: a comprehensive Python-based system for macromolecular structure solution. *Acta Crystallogr. D Biol. Crystallogr.* **66,** 213–221 CrossRef Medline
38. Sheldrick, G. M. (2008) A short history of SHELX. *Acta Crystallogr. A* **64,** 112–122 CrossRef Medline
39. Kabsch, W. (2010) XDS. *XDS. Acta Crystallogr. D Biol. Crystallogr.* **66,** 125–132 CrossRef Medline
40. Emsley, P., and Cowtan, K. (2004) Coot: model-building tools for molecular graphics. *Acta Crystallogr. D Biol. Crystallogr.* **60,** 2126–2132 CrossRef Medline
41. Collaborative Computational Project, Number 4 (1994) The CCP4 suite: programs for protein crystallography. *Acta Crystallogr. D. Biol. Crystallogr.* **50,** 760–763 CrossRef Medline
42. Davis, I. W., Murray, L. W., Richardson, J. S., and Richardson, D. C. (2004) MolProbity: structure validation and all-atom contact analysis for nucleic acids and their complexes. *Nucleic Acids Res.* **32,** W615–W619 CrossRef Medline
43. Studier, F. W. (2005) Protein production by auto-induction in high density shaking cultures. *Protein Expr. Purif.* **41,** 207–234 CrossRef Medline

A step-by-step *in crystallo* guide to bond cleavage and 1,6-anhydro-sugar product synthesis by a peptidoglycan-degrading lytic transglycosylase

Allison H. Williams, Richard Wheeler, Lesly Rateau, Christian Malosse, Julia Chamot-Rooke, Ahmed Haouz, Muhamed-Kheir Taha and Ivo Gomperts Boneca

J. Biol. Chem. 2018, 293:6000-6010.
doi: 10.1074/jbc.RA117.001095 originally published online February 26, 2018